Available online at www.sciencedirect.com
SCIENCE DIRECT®
Coordination Chemistry Reviews 249 (2005) 2677–2690
COORDINATION CHEMISTRY REVIEWS
www.elsevier.com/locate/ccr

Review

Polynuclear manganese grids and clusters—A magnetic perspective

Laurence K. Thompson [a,*], Oliver Waldmann [b], Zhiqiang Xu [a]

[a] *Department of Chemistry, Memorial University, St. John's, Nfld, Canada A1B 3X7*
[b] *Department of Chemistry and Biochemistry, University of Bern, Freiestrasse 3, CH-3012 Bern, Switzerland*

Available online 19 August 2005

Contents

Abstract

High nuclearity paramagnetic, spin-coupled transition metal clusters and grids are fascinating chemists and physicists partly because of their structural beauty, and the challenge of creating them, but also because of their novel physical properties. Magnetic interactions between the spin centers are a primary focus. This review will examine a selection of Mn(II) polynuclear grids and clusters, with nuclearities in the range Mn_4 to Mn_9. Theoretical treatments of the magnetic properties are discussed, and approaches to solving the exchange problem for 'large' spin systems related to computational difficulties. A freely available software package (MAGMUN4.1) is presented as a means of dealing simply with spin-coupled clusters in general, and symmetry reduction methods are discussed briefly as a means of dealing with 'large' spin systems.

Keywords: Grids; Clusters; Magnetic exchange; Exchange coupling schemes; Software; Large spin systems

* Corresponding author. Tel.: +1 709 737 8750; fax: +1 709 737 3702.
E-mail address: lthomp@mun.ca (L.K. Thompson).

0010-8545/$ – see front matter © 2005 Elsevier B.V. All rights reserved.
doi:10.1016/j.ccr.2005.07.002

1. Introduction

Polynuclear coordination complexes with metal ions in intramolecular spin communication have caught the imagination of synthetic and theoretical chemists alike, and have been a focal topic among chemists and physicists with mutual interests in the emerging area of 'molecular magnetism'. While a primary interest within this community rests with the creation of molecules with magnetic memory, with applications at the molecular level as a target, such examples are rare. As a result the creative instincts of synthetic chemists have been piqued to provide synthetic ways of assembling molecules with large numbers of magnetic subunits connected by bridging groups, which provide magnetic (spin) communication within a single molecular entity. A number of magnetically bistable, low temperature nanomagnets have been produced with examples of Mn_{12} [1], Mn_{18} [2], Mn_{22} [3] and Mn_{30} [4] clusters, containing mixtures of Mn(II), Mn(III) and Mn(IV) centers. However, it is difficult to produce such systems by design.

An effective approach to 'specific' high nuclearity systems is to use a 'self assembly' technique. This involves the encoding of coordination information in a ligand in the form of suitably disposed coordination pockets, which then interact with a transition metal ion. The metal ion reads the coordination information in terms of its own stereochemical and bonding preferences, and if there is an appropriate information match, a self-assembled structure results. High nuclearity systems, particularly $[n \times n]$ grids, have been produced successfully by this approach, with a significant degree of predictability.

In this review, polynuclear manganese(II) complexes of a series of polytopic picolinic-hydrazone ligands will form the focus of discussion of the magnetic exchange problem in systems with moderate nuclearity ($M_{4–9}$), and the limits of dealing with these 'large' spin systems will be brought into focus in relation to the magnitude of the spin state matrix calculations, and software and computer capabilities. Previous reviews have dealt with some aspects of the magnetic properties of grids in this class involving a variety of metal ions [5–7].

Tetradentate hydrazone ligands, e.g. poap (Fig. 1) have several different coordination modes, with the most common involving metal ion bridging through hydrazone oxygen and diazine nitrogen groups (Fig. 1a–c). Mn(II), Co(II), Cu(II), Ni(II) and Zn(II) salts react with ligands in this class to produce mainly square heteroleptic $[2 \times 2]$ grid complexes (Scheme 1), in which four metal ions self-assemble in the presence of four tetradentate ligands to form the grid [8,9]. The ligands fill five donor sites per metal, which requires four extra mono-dentate ligands to complete the six coordination requirement for the four octahedral M(II) ions [8]. Another oligomeric possibility is a self-assembled homoleptic cluster involving six ligands and five six-coordinate metal ions (30 sites for each), and this is achieved for Mn(II), Co(II) and Zn(II) examples, where the anion involved has a low

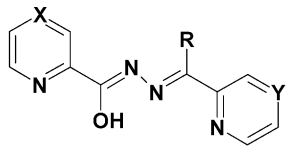

poap (X=Y=CH, R=NH_2), pzoap (X=N,Y=CH, R=NH_2), poapz (X=CH, Y=N, R=NH_2),pzoapz (X=Y=N, R=NH_2), pomp (X=Y=CH, R=CH_3).

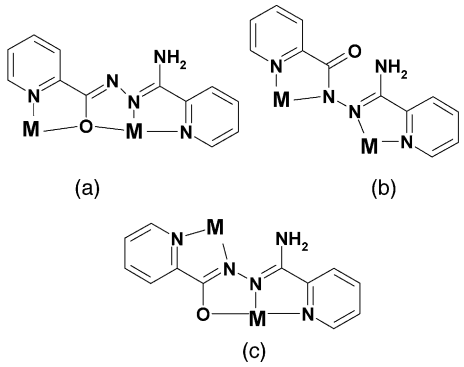

Fig. 1. Ditopic picolyl hydrazone ligands, and their different coordination modes.

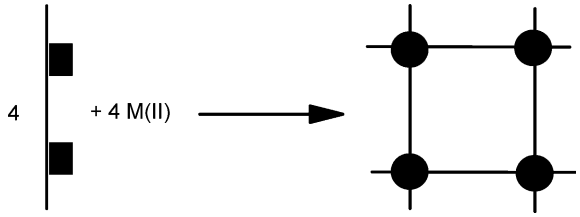

Scheme 1. Self-assembly mechanism for a $[2 \times 2]$ grid using a ditopic ligand.

coordination capacity, e.g. perchlorate [10,11]. Heptadentate tritopic ligands, e.g. 2poap and its derivatives (Fig. 2), self assemble in high yield to produce $[3 \times 3]$ square grid complexes (Scheme 2) involving nine six-coordinate metal ions and six ligands with a $[M_9–(\mu\text{-}O)_{12}]$ hydrazone oxygen bridged core structure (M = Mn(II), Fe(III), Ni(II), Co(II), Cu(II), Zn(II)) [12–20]. The $Mn(II)_9$ complexes display rich electrochemistry, with four Mn(II) ions oxidizing readily to produce mixed oxidation state Mn(II)/Mn(III) grids, with reduced electron content [12,20].

All of the polynuclear manganese complexes involve metal ions bridged by oxygen groups with large Mn–O–Mn bridge angles (>125°), leading to intramolecular antiferro-

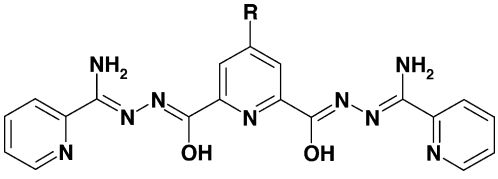

R = H (2poap); R = Cl, OMe, SR'

Fig. 2. Selection of tritopic picolyl hydrazone ligands.

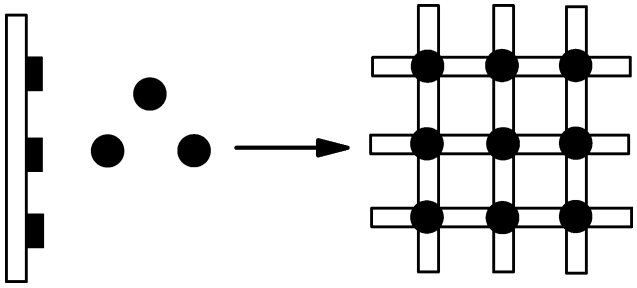

Scheme 2. Self-assembly mechanism for a [3 × 3] grid using a tritopic ligand.

magnetic exchange. The exchange situation can be dealt with using a simple Kambe approach [21] to calculate the total spin states (S') and their energies for the Mn_4 and Mn_5 examples, but the complexity of the exchange situation for the Mn_9 systems requires a different approach. Examples within each class will be discussed in terms of the most appropriate methodology. A generalized software package built on a Windows™ platform (MAGMUN4.1) [22] will be discussed, which has general applicability for a wide variety of cluster models.

2. MAGMUN4.1

2.1. Generalized exchange hamiltonian

High nuclearity metal ion assemblies can be assessed in terms of a generalized spin Hamiltonian, which can include interactions among all the spin centers, effects of the ligand fields and Zeeman splitting terms (Eq. (1)).

$$H = -\sum_{i<j} J_{ij} \cdot S_i \cdot S_j + \sum_i S_i \cdot D_i \cdot S_i + \mu_B \sum_i S_i \cdot g_i \cdot B \quad (1)$$

$$\chi_M = \frac{N\beta^2 g^2}{3kT} \frac{\sum S'(S'+1)(2S'+1)\, e^{-E(S')/kT}}{\sum (2S'+1)\, e^{-E(S')/kT}} \quad (2)$$

In an isotropic spin only situation, ignoring the ligand field term $\sum_i S_i \cdot D_i \cdot S_i$, and assuming identical and isotropic g factors for all spin centres, the molar susceptibility can be calculated using the general form of the Van Vleck equation (Eq. (2)), for a particular temperature range. S' specifies the total spin angular momentum, resulting from a summation of the spin angular momenta of all the individual ions of spin S. $E(S')$ represents the energy of a particular state derived as a function of J_{ij}.

The dimension of the Hamiltonian matrix grows enormously with increasing number of spin centers, and spin quantum numbers (S), and an exact diagonalization of the matrix quickly exceeds the capabilities of any computer. However, within normal computer limits (e.g. 1 GB RAM), quite large calculations are possible.

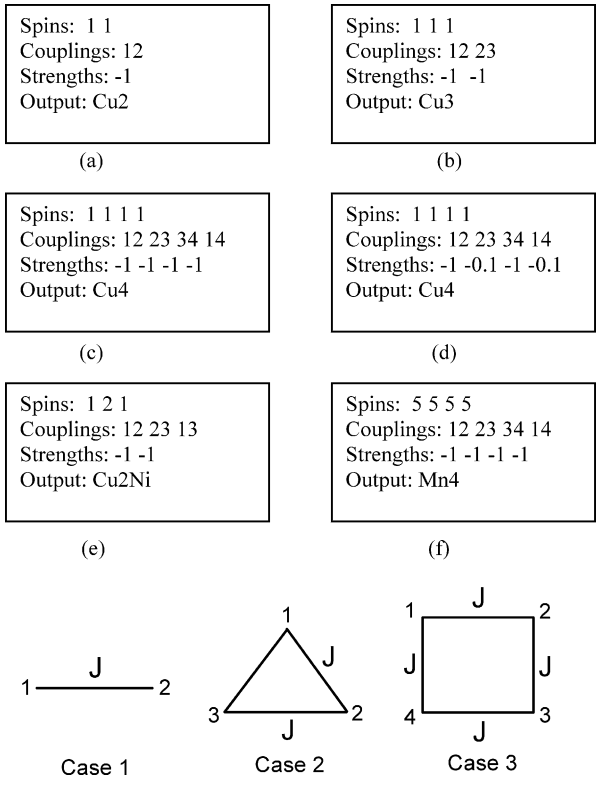

Fig. 3. Input file models for dinuclear, trinuclear and tetranucler spin systems for the calculation of *.spk files for use with MAGMUN4.1.

2.2. Using MAGMUN4.1

MAGMUN4.1 [22] provides a convenient platform to model the magnetic properties of both simple and complex polynuclear spin structures, without the necessity for deriving exchange equations, which in some cases can be non-trivial, or of defining the eigenstates of the exchange problem directly. The spin state and energy calculations are carried out after first of all defining the spin model, and summarizing the exchange information from the model in an input file (OW01.ini). Some simple spin models are shown in Fig. 3 for dinuclear (a; case 1), trinuclear (b; case 2) and tetranuclear (c; case 3) examples. Atoms are defined numerically in the model, and J values assigned in the normal way. Input files are shown for each case with equivalent J values for each connection. The spins are input in line 1 (any value of S expressed as integer spins), the coupling scheme in line 2 (e.g. 12, 23, etc., refer to connectivity between coupled atoms 1–2, 2–3, etc.), the exchange energy is entered in line 3 for each exchange connection specified (any value plus or minus can be input in cm^{-1}), and line 4 assigns the output file name. In a system in which all the J values are considered to be the same, either through direct symmetry or imposed symmetry, an entry of '−1' as the exchange energy is conveniently translated into a 'J' factor in the non-linear regression analysis of the experimental data (vide infra). Alternatively individual 'J' values can be input to define specific exchange connections, thus allowing considerable flexibility with the exchange energy

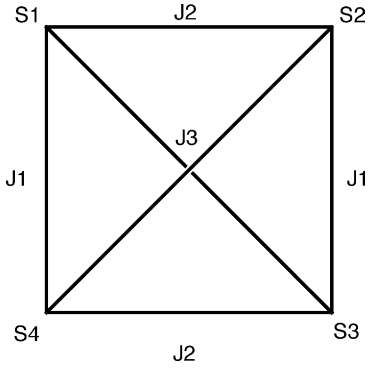

Fig. 4. General exchange coupling model for tetranuclear grid based systems.

profile, and variations in J within the same molecular entity. Also equivalent groups of exchange integrals can be dealt with by expressing them in the form of a ratio of J values; for example in Case 3 J_{23} and J_{14} could be represented as −0.1 (Fig. 3d) to indicate that after the non-linear regression analysis of the experimental data the absolute J values will be related by a ratio of 1:10. Different spin states (i.e. different metal ions or mixed oxidation state species) can also be input in line 1 (e.g. Fig. 3e represents a Cu_2Ni symmetric linear trinuclear system with no 1–3 coupling). Models are not confined to 2D polygons, and three dimensional polyhedral systems are dealt with in the same way.

Complex cases, e.g. a square model with three different J values (Fig. 4; $J1 \neq J2 \neq J3$), can be fitted in terms of some 'fixed' ratio of input energies, e.g. −1, −0.5, −0.1, which would generate a ratio 1:0.5:0.1, respectively. Individual 'J' values cannot be evaluated directly with the current package.

After the input file (OW0L.ini) has been written, the file containing the profile of spin states (S') and their energies (***.spk) is generated using the program OW01.exe. The .spk file can then be processed within the menu driven subroutines available in MAGMUN4.1 to simulate magnetic profiles, and fit the experimental data using built in non-linear regression routines. The fitted results can be saved directly or exported to a spread sheet. Magnetization versus field profiles can also be generated and fitted using standard Brillouin functions and fitting routines. A tutorial is included in the program, which highlights the essential features of MAGMUN4.1.

3. [2 × 2] Mn grids

Examples of [2 × 2] $Mn(II)_4$ grids are rare. The molecular structure of the complex $[Mn_4(poapz\text{-}H)_4(H_2O)_4](NO_3)_4{\cdot}H_2O$ (**1**) is shown in Fig. 5. Two pairs of parallel ligands form an asymmetric arrangement above and below the Mn_4–(μ-O)$_4$ plane. Mn–Mn distances fall in the range 3.91–3.97 Å, with Mn–O–Mn angles in the range 127.9–129.3°. Six-coordination is completed at Mn(1) and Mn(3) with four water molecules [9].

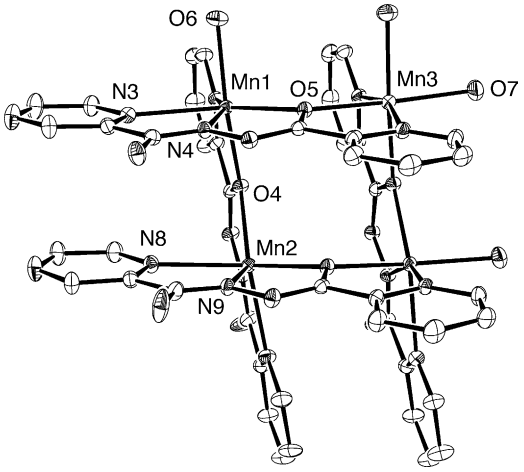

Fig. 5. Structural representation of $[Mn_4(poapz\text{-}H)_4(H_2O)_4](NO_3)_4{\cdot}H_2O$ (**1**) (reprinted from Ref. [9]).

3.1. Magnetic properties of M_4 [2 × 2] grids

In a general case a square (D_{4h}) or distorted square (D_{2d}) [2 × 2] grid can be described by an exchange coupling scheme involving three exchange integrals ($J1$, $J2$, $J3$) according to the appropriate Hamiltonian expression (Eq. (3)) (Fig. 4).

$$H_{ex} = -J1\{S_2 \cdot S_3 + S_1 \cdot S_4\} - J2\{S_1 \cdot S_2 + S_3 \cdot S_4\} - J3\{S_1 \cdot S_3 + S_2 \cdot S_4\} \quad (3)$$

$J1$ is the exchange along the vertical sides and $J2$ along the horizontal sides of the square. In most cases diagonal terms ($J3$) can be set to zero because cross-coupling terms are assumed to be small or insignificant. Using the conventional spin-vector coupling model [21,23], eigenvalues of Eq. (3) can be obtained analytically for a D_{4h} [2 × 2] grid with $J = J1 = J2$ and $J3 = 0$. The eigenvalues are then given by Eq. (4),

$$E(S', S_{13}, S_{24}) = \frac{-J}{2}[S'(S'+1) - S_{13}(S_{13}+1) - S_{24}(S_{24}+1)] \quad (4)$$

where $S_{13} = S_1 + S_3$; $S_{24} = S_2 + S_4$; $S' = S_1 + S_2 + S_3 + S_4$.

Another coupling situation which arises in the limit $J1 = J3 = 0$ is that of a "dimer of dimers" (Eq. (5); see Fig. 4 for model), corresponding to the general Hamiltonian

$$H_{ex} = -J2\{S_1 \cdot S_2\} - J2'\{S_3 \cdot S_4\} \quad (5)$$

where the horizontal coupling strengths might assume different values $J2$ and $J2'$. Using the same method the eigenvalues are obtained as (Eq. (6))

$$E(S', S_{12}, S_{34}) = \frac{-J2}{2}[S_{12}(S_{12}+1)] - \frac{J2'}{2}[S_{34}(S_{34}+1)] \quad (6)$$

with $S_{12} = S_1 + S_2$; $S_{34} = S_3 + S_4$ and $S' = S_{12} + S_{34}$. All these results are valid for arbitrary values of the spin quantum numbers S_i ($i = 1, \ldots, 4$).

Using the addition rules for spin vectors the allowed values for S', and S_{13}, S_{24}, or S_{12}, S_{34}, respectively can be obtained. By substituting the appropriate energy terms into the modified van Vleck equation (Eq. (7); $E_{(S')}$ refers to the energy of each spin state

$$\chi_M = \frac{N\beta^2 g^2}{3k(T-\theta)} \frac{\sum S'(S'+1)(2S'+1)\, e^{-E(S')/kT}}{\sum (2S'+1)\, e^{-E(S')/kT}} (1-\rho) + \frac{N\beta^2 g^2 S(S+1)\rho}{3kT} + \text{TIP} \quad (7)$$

defined by S'), the susceptibility values can be computed for a particular temperature range. In practice this can be achieved by the use of simple programming techniques whereby iterative procedures span the required S' values for fitted values of J in routines that allow regression of the experimental data against Eq. (7). Best fit values of g and J are thus obtained, allowing for paramagnetic impurity (fraction ρ), temperature independent paramagnetism (TIP), and a Weiss-like corrective term (θ) to deal with small intermolecular exchange effects. A comprehensive review by Murray [24] deals more generally with the magnetic properties of tetranuclear complexes.

The [2 × 2] Mn(II) grid **1** can be considered as a simple case (Eq. (3)), in which $S_{1-4} = 5/2$, for $J = J1 = J2$ and $J3 = 0$. Using the Kambe vector coupling scheme [21] a total of 146 energy states are calculated, with the largest matrix dimension being 24. A plot of S' against relative energy for $J = -1\ \text{cm}^{-1}$ (antiferromagnetic case) is shown in Fig. 6, with S' values varying from 0 to 10 in integer steps, as expected for a system with an even number of spin centers. Exchange equations can also be derived directly for this system, using the S' values and energies based on J, and standard approaches used to fit the experimental data using commercial software or in house programs. However, a much simpler approach is to use MAGMUN4.1 (vide supra) [22]. In the first step the

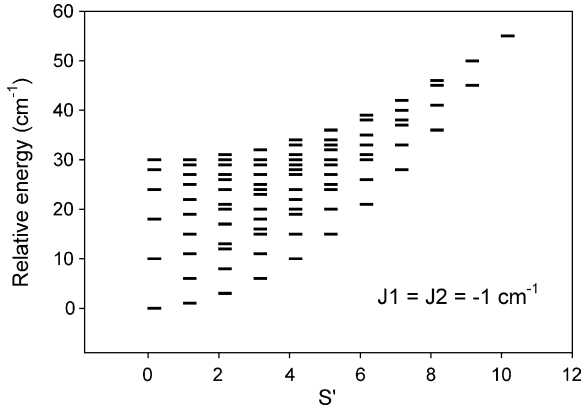

Fig. 6. Spin state energy spectrum for a Mn(II)$_4$ [2 × 2] grid with $J1 = J2 = -1\ \text{cm}^{-1}$.

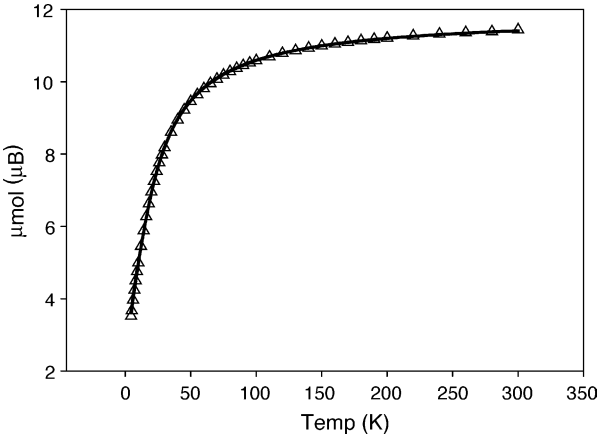

Fig. 7. Plot of magnetic moment per mole as a function of temperature for $[Mn_4(poapz\text{-}H)_4(H_2O)_4](NO_3)_4 \cdot H_2O$ (**1**). The solid line represents the best fit of the experimental data to Eq. (8) for $g = 2.001(1)$, $J = -2.77(1)\ \text{cm}^{-1}$ [9].

energy spectrum (S', E) is calculated with an input J value (e.g. $-1\ \text{cm}^{-1}$), and stored as the input ***.spk file. The χ/T (or μ/T) profile is then calculated, and compared visually with the experimental data by scaling the J value, and entering values for 'g' and other parameters (TIP, θ, ρ) as required. Regression of the experimental data is then carried out with iterations based on reasonably guessed fitting parameters.

3.2. Magnetic properties of $[Mn_4(poapz\text{-}H)_4(H_2O)_4](NO_3)4 \cdot H_2O$ (*1*)

The variable temperature magnetic data for **1** are shown in Fig. 7 as a plot of magnetic moment per mole as a function of temperature. The moment drops smoothly from 11.4 μ_B at 300 K to 3.5 μ_B at 4.5 K, indicative of intramolecular antiferromagnetic exchange [9]. The moment approaches zero, expected for an even numbered grid in the low temperature antiferromagnetic limit. The data were fitted using Eqs. (7) and (8), and MAGMUN4.1 [22], to give $g = 2.001(1)$, $J = -2.77(1)\ \text{cm}^{-1}$, TIP = 0 $\text{cm}^3\ \text{mol}^{-1}$, $\rho = 0.04$,

$$H_{ex} = -J\{S_1 \cdot S_2 + S_2 \cdot S_3 + S_3 \cdot S_4 + S_1 \cdot S_4\} \quad (8)$$

$\theta = 0$ K ($10^2 R = 0.36$; $R = [\sum (\chi_{obs.} - \chi_{calc.})^2 / \sum \chi^2_{obs.}]^{1/2}$. This result is in good agreement with a previously determined fit [9].

4. Trigonal bipyramidal clusters

The tetradentate hydrazone ligands (Scheme 1) have been shown to self-assemble with certain Mn(II), Co(II) and Zn(II) salts to produce homoleptic, trigonal bipyramidal clusters. This usually occurs when the anion has weak coordination capacity, and does not compete successfully for the metal coordination sites as the cluster forms [10,11]. The structure of $[Mn_5(poap\text{-}H)_6](ClO_4)_4 \cdot 3.5MeOH \cdot H_2O$ (**2**) is shown in

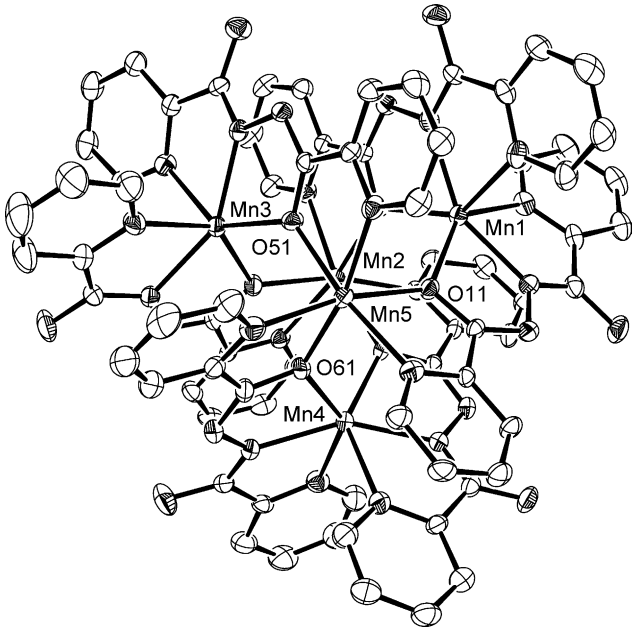

Fig. 8. Structural representation of $[Mn_5(poap\text{-}H)_6](ClO_4)_4 \cdot 3.5MeOH \cdot H_2O$ (**2**) (reprinted from Ref. [10]).

Fig. 8 looking down the 'trigonal' axis. The core structure is shown in Fig. 9, highlighting the hydrazone oxygen bridging interactions. Mn(2) and Mn(5) are the apical metal centers, which are connected to the three equatorial Mn(II) ions by the bridging oxygen atoms only. Mn–Mn separations fall in the range 3.90–3.97 Å, with Mn–O–Mn angles in the range 128–131°. These dimensions are similar to those observed in the square [2 × 2] Mn_4 grid.

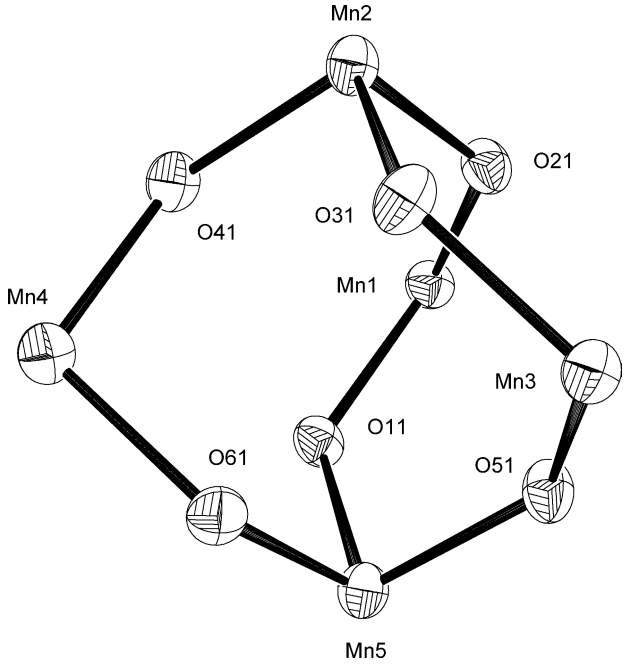

Fig. 9. Core structural representation for **2**.

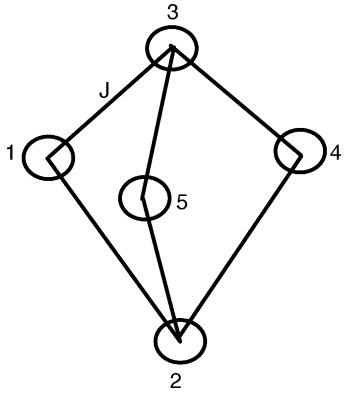

Fig. 10. Spin exchange model for trigonal bipyramidal cluster.

4.1. Magnetic properties of the Mn(II)$_5$ trigonal bipyramid

The magnetic exchange model for **2** (Fig. 10) involves six exchange pathways, which for simplicity may be regarded as equal, based on the structure. The vector coupling scheme for this trigonal bipyramidal model may be summarized using exchange Hamiltonian (Eq. (9)), and the subsequent equations,

$$\begin{aligned} H_{ex} &= -J\{S_1 \cdot S_3 + S_4 \cdot S_3 + S_5 \cdot S_3 + S_1 \cdot S_2 \\ &\quad + S_2 \cdot S_5 + S_2 \cdot S_4) \\ &= -J\{S_3 \cdot (S_1 + S_4 + S_5) + S_2 \cdot (S_1 + S_4 + S_5)\} \\ &= -J\{S_2 + S_3) \cdot (S_1 + S_4 + S_5)\} \\ &= -J(S_{23} \cdot S_{145}) \\ &= \{-J/2\}(S'^2 - S_{23}^2 - S_{145}^2) \end{aligned} \quad (9)$$

where $S_{23} = S_2 + S_3$; $S_{15} = S_1 + S_5$; $S_{145} = S_{15} + S_4$; $S' = S_{23} + S_{145}$.

The eigenvalues are $E(S', S_{23}, S_{145}) = \{-J/2\}[S'(S'+1) - S_{23}(S_{23}+1) - S_{145}(S_{145}+1)]$.

The allowed values of S', S_{23} and S_{145}, and their appropriate energies are substituted into the van Vleck equation in the usual way to create a susceptibility profile as a function of temperature. The procedure of generating the exchange equation itself for such a large system presents a somewhat daunting task, and so the use of MAGMUN4.1, or e.g. MAGPACK (MAGPACK includes both isotropic and anisotropic exchange terms, and single ion anisotropic effects [25,26]) is a really attractive alternative method.

The S' energy spectrum, calculated using MAGMUN4.1, is illustrated in Fig. 11. The largest matrix dimension is 120 ($S' = 7/2$), with a total dimension (total number of energy states) of 780. What is interesting is the fact that the lowest calculated S' value is 5/2, which would allow us to predict an $S' = 5/2$ ground state. The variable temperature magnetic moment data for $[Mn_5(poap\text{-}H)_6](ClO_4)_4 \cdot 3.5MeOH \cdot H_2O$ (**2**) are shown in Fig. 12. The moment drops from 12.5 μ_B (per mole) at 300 K to 5.7 μ_B at 2 K, indicative of intramolecular antiferromag-

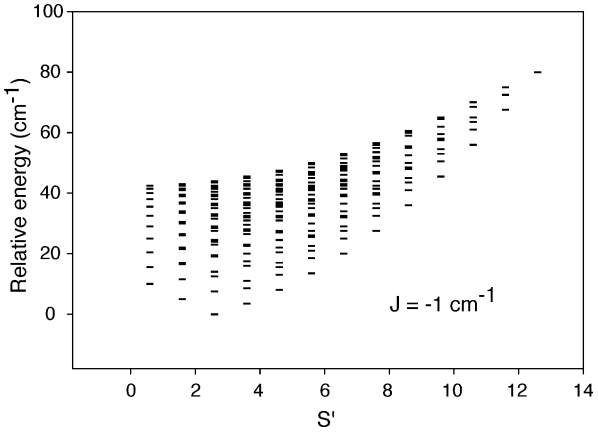

Fig. 11. Spin state energy spectrum for a $Mn(II)_5$ trigonal bipyramidal cluster with $J = -1\ cm^{-1}$.

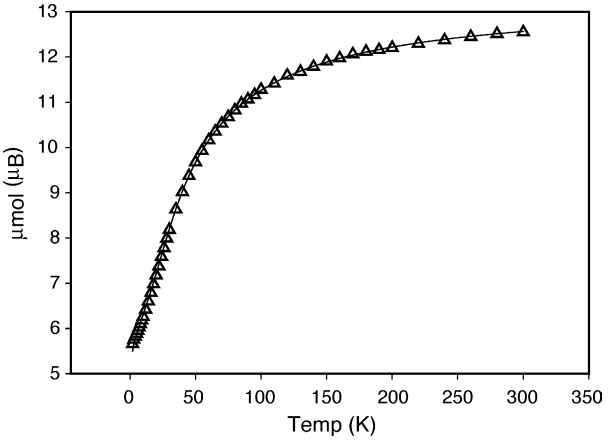

Fig. 12. Plot of magnetic moment per mole as a function of temperature for $[Mn_5(poap\text{-}H)_6](ClO_4)_4{\cdot}3.5MeOH{\cdot}H_2O$ (**2**). The solid line represents the best fit of the experimental data to Eq. (9) for $g = 2.010(4)$, $J = -3.4(4)\ cm^{-1}$ [11].

netic exchange. The low temperature value suggests an $S' = 5/2$ ground state. The data were fitted to the exchange Hamiltonian (Eq. (9)) for a trigonal bipyramidal arrangement of $S = 5/2$ spin centers arranged according to Fig. 10, within MAGMUN4.1. An excellent fit gave $g = 2.010(4)$, $J = -3.4(4)\ cm^{-1}$, $\rho = 0.005$, TIP = 0 $cm^3\ mol^{-1}$, $\theta = -0.4$ K, $10^2R = 0.45$. The solid line in Fig. 12 is calculated with these parameters. Magnetization versus field data at 2 K are consistent with the $S' = 5/2$ ground state [11].

5. [3 × 3] Nona-nuclear grids

5.1. $Mn(II)_9$ '45 electron' grids

Tritopic picolinic dihydrazone ligands (Fig. 2) have proven to be classic examples of ligands which can be prepared simply, and encoded readily with coordination information necessary to promote self-assembly. $Mn(II)_9$ self assembled [3 × 3] grids form readily and in high yield (Scheme 2)

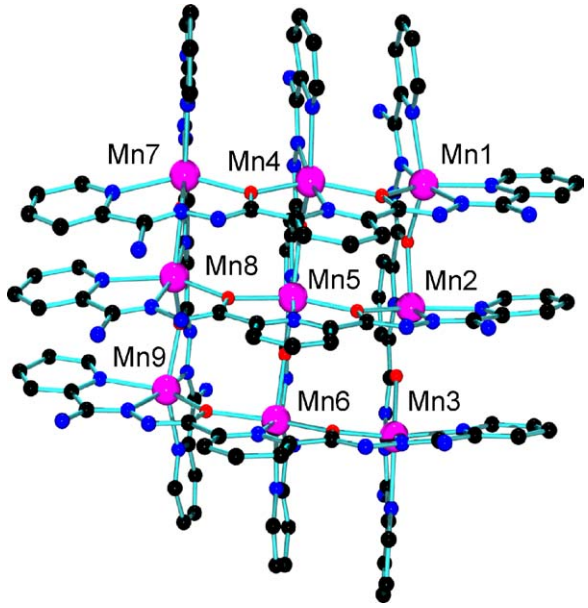

Fig. 13. Structural (POVRAY©) representation of $[Mn_9(2poap\text{-}2H)_6](ClO_4)_6{\cdot}3.6CH_3CN{\cdot}H_2O$ (**3**) [12].

[6,12–20]. The ligands can be easily functionalized to take advantage of variable electronic effects (e.g. R = H, Cl, OMe), which have a pronounced influence on electrochemical properties, and also provide tethers for surface binding applications (gold; R = Cl, SEt, SMe) [19].

The structure of a typical $Mn(II)_9$ grid complex $[Mn_9(2poap\text{-}2H)_6](ClO_4)_6{\cdot}3.6CH_3CN{\cdot}H_2O$ (**3**) is shown in Fig. 13, and the core structure is illustrated in Fig. 14. Six ligands encompass the square grid core arrangement of nine Mn(II) ions bridged by twelve deprotonated hydrazone oxygen atoms. Mn–Mn distances are in the range 3.9–4.0 Å, with

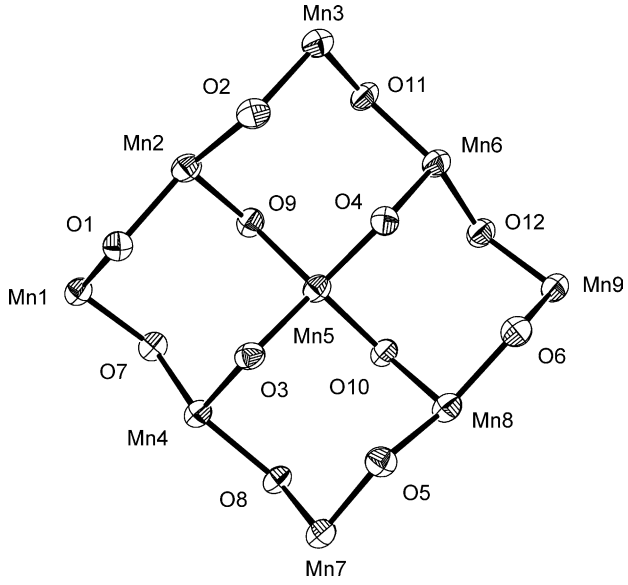

Fig. 14. Core structural representation for **3**.

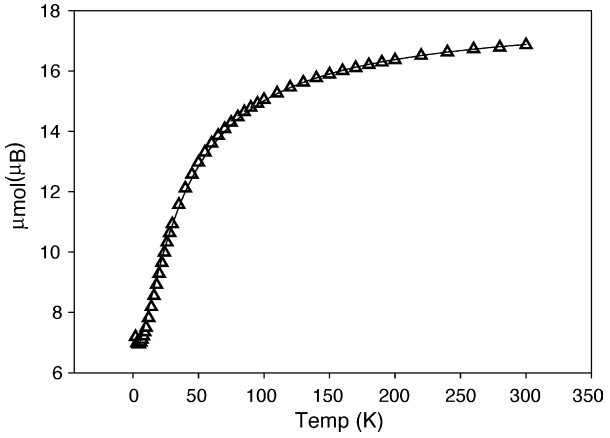

Fig. 15. Plot of magnetic moment per mole as a function of temperature for $[Mn_9(2poap\text{-}2H)_6](ClO_4)_6{\cdot}3.6CH_3CN{\cdot}H_2O$ (**3**). The solid line represents the best fit of the experimental data to Eq. (10) for $g = 2.0$, $J1 = -3.8\,cm^{-1}$, $J2 = 0\,cm^{-1}$ [15].

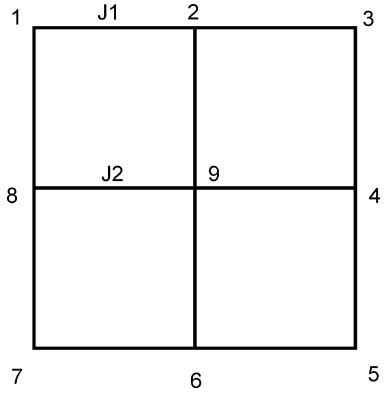

Fig. 16. Spin exchange model for [3 × 3] nona-nuclear grid.

Mn–O–Mn angles in the range 126.6–130.0° [12]. A plot of $\mu_{mol}/(T)$ for **3** is illustrated in Fig. 15. The moment drops from 16.9 to 6.4 μ_B at 4 K. This behavior is consistent with the presence of significant antiferromagnetic coupling within the grid, with a room temperature moment consistent with nine high spin Mn(II) centers, and a low temperature moment close to what would be expected for one 'uncoupled' Mn(II) center, i.e. an $S' = 5/2$ ground state. Other $Mn(II)_9$ grids in this class behave in exactly the same fashion. Magnetization data as a function of field at 1.8 K confirm this for **3** [15], with a good fit to the appropriate Brillouin function for an $S' = 5/2$ spin system in the range 0–3 T. An isotropic exchange model for this type of grid (Eq. (10); Fig. 16) should include

$$H_{ex} = -J1\{S_1 \cdot S_2 + S_2 \cdot S_3 + S_3 \cdot S_4 + S_4 \cdot S_5 + S_5 \cdot S_6 + S_6 \cdot S_7 + S_7 \cdot S_8 + S_1 \cdot S_8\} - J2\{S_2 \cdot S_9 + S_4 \cdot S_9 + S_6 \cdot S_6 + S_8 \cdot S_9\} \quad (10)$$

two exchange integrals, and a full spin Hamiltonian should also include dipole–dipole terms, second order ligand field terms and Zeeman terms. Such an analysis is impeded by the enormous dimensions of a typical calculation (vide infra), and in order to simplify the exchange situation the grid can be considered in the simple isotropic limit as the sum of a ring of eight Mn(II) centers (atoms 1–8; Fig. 16), coupled to the central Mn(II) ion (atom 9; Fig. 16). Since the magnetic properties of the system are clearly dominated by antiferromagnetic exchange, and since the ground state is $S' = 5/2$, it is reasonable to assume that $J1$ is negative and dominates the exchange situation, and that $J2$ can effectively be ignored. The data for **3** have been successfully fitted to an isotropic exchange model based on Fig. 16, with $g = 2.0$, $J1 = -3.8\,cm^{-1}$, $J2 = 0\,cm^{-1}$ [15]. The solid line in Fig. 15 corresponds to these fitted parameters for **3**. $J1$ values for all compounds in this class are similar, and are comparable with the exchange integral found for the $[Mn_4(\mu\text{-}O)_4]$ square grid complex $[Mn_4(poapz\text{-}H)_4(H_2O)_4]\,(NO_3)_4{\cdot}H_2O$ (**1**) ($J = -2.85\,cm^{-1}$) [9], in keeping with the similar structural elements present in both systems.

A simpler alternative approach is to consider the outer ring of eight Mn(II) centers as an isolated chain, which is reasonable for a chain length of eight spin centers, and assume that there is effectively no coupling between the ring (chain) and the central Mn(II) ion. This can be accomplished using the Fisher model (Eqs. (11) and (12)) for an $S = 5/2$ chain [27], where the large local spin ($S = 5/2$) is treated as a classical vector.

$$\chi_{Mn} = \frac{Ng^2\beta^2 S(S+1)}{3kT}\frac{(1+u)}{(1-u)} \quad (11)$$

$$u = \coth\left[\frac{JS(S+1)}{kT}\right] - \left[\frac{kT}{JS(S+1)}\right] \quad (12)$$

$$\chi_{mol} = \left[\frac{(8\chi_{Mn} + 1.094g^2)}{(T-\theta)}\right](1-\alpha) + \left(\frac{1.094g^2}{T}\right)\alpha + TIP \quad (13)$$

The complex $[Mn_9(2poap\text{-}2H)_6](C_2N_3)_6{\cdot}10H_2O$ (**4**) [19] has a comparable structure to **3**, with Mn–Mn distances in the range 3.886–3.923 Å, and Mn–O–Mn angles in the range 126.7–126.9°. The variable temperature magnetic profile for **4** is very similar to that of **3**, with a low temperature moment indicative of an $S' = 5/2$ ground state. The magnetic data for **4** were fitted to Eqs. (11)–(13), with the susceptibility scaled for eight spin-coupled Mn(II) centers in a chain, and corrected for temperature independent paramagnetism (TIP), paramagnetic impurity fraction (α), intermolecular exchange effects (θ—Weiss like temperature correction), and the central, 'isolated' Mn(II) center (Eq. (13)). A good data fit for **4** gave $g = 2.028$, $J = -4.7\,cm^{-1}$, $\alpha = 0.001$, $TIP = 0\,cm^3\,mol^{-1}$, $\theta = 0$ K ($10^2R = 1.9$; $R = [\sum(\chi_{obs.} - \chi_{calc.})^2 / \sum \chi^2_{obs.}]^{1/2}$) [19]. The data are well reproduced over the whole temperature range indicating that the chain model is reasonable down to 2 K, and that the assumption that $J2$ can be ignored is not unreasonable. While

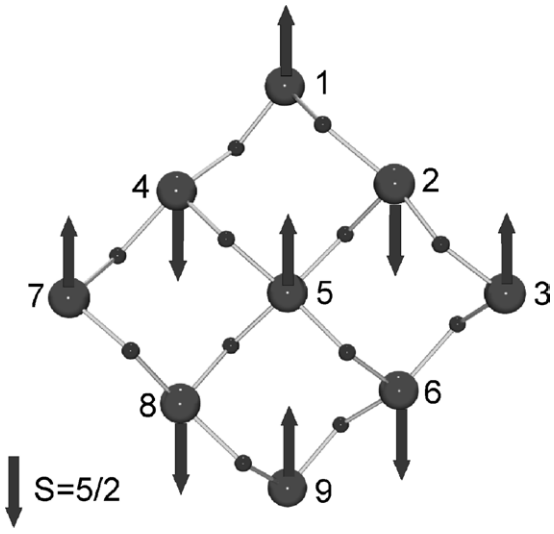

Fig. 17. Spin dipole model for an anti-ferromagnetically coupled $Mn(II)_9$ [3 × 3] grid.

the data fit is good in this case, and the result is consistent with the ring model for **4** and other related systems, some doubt should be expressed concerning the assumption that $J2 = 0\ cm^{-1}$. In fact inelastic neutron scattering experiments, and low temperature high-field torque measurements indicate that $J1 \approx J2$ [28]. A general spin model for the $Mn(II)_9$ grids is shown in Fig. 17, with an alternation of Mn(II) $S = 5/2$ dipoles around the ring (chain) creating an effective $S' = 0$ ground state at low temperatures, thus resulting in an $S' = 5/2$ ground state overall when the central manganese atom is included.

6. Mixed oxidation state Mn(II)/Mn(III) grids

*6.1. $[Mn(III)_3Mn(II)_6(Cl2poap\text{-}2H)](ClO_4)_9\cdot 7H_2O$ (**6**), $[Mn(III)_4Mn(II)_5(2poap\text{-}2H)](ClO_4)_{10}\cdot 10H_2O$ (**7**)*

The $Mn(II)_9$ grids show a remarkable ability to undergo reversible oxidation and reduction, both electrochemically and chemically, to produce Mn(II)/Mn(III) derivatives. The complex $[Mn_9(Cl2poap\text{-}2H)_6](ClO_4)_6\cdot 8H_2O$ (**5**) (Cl2poap; Fig. 2, R = Cl) [17] has a similar structure to **3**, and exhibits rich electrochemistry, with a quasi-reversible wave in cyclic voltammetry (Fig. 18) at $E_{1/2} \approx 0.7$ V ($\Delta E_p = 216$ mV) (versus Ag/AgCl), corresponding to a four electron redox process, followed by three one-electron, more reversible waves at higher potential (1.1–1.6 V) [17]. Differential pulse voltammetry (DPV) (Fig. 19) shows these events much more clearly, and reveals a fourth high potential wave. The first wave is associated with the oxidation of the four corner Mn(II) centers to Mn(III), while the higher potential sequence of four one-electron waves is associated with oxidation of the four Mn(II) centers on the sides of the grid to Mn(III). Compound **3** exhibits similar electrochemical responses, but with four clearly defined one-electron waves [12,20].

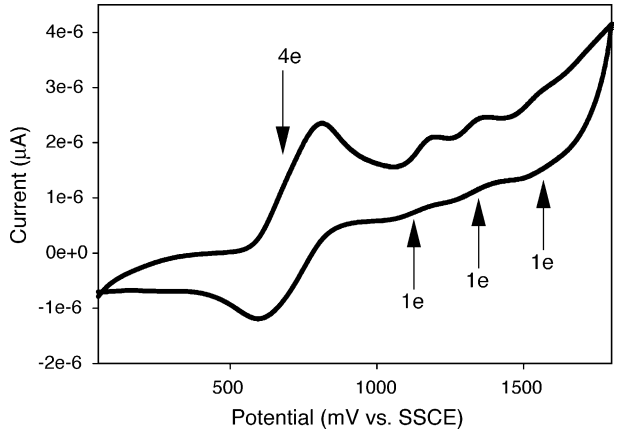

Fig. 18. Cyclic voltammetry (CH_3CN vs. Ag/AgCl) for $[Mn_9(Cl2poap\text{-}2H)](ClO_4)_6\cdot 8H_2O$ (**5**).

The possibility of isolating Mn(II)/Mn(III) grids, with the potential for novel magnetic properties, prompted us to explore means of producing such derivatives. Chemical oxidants with oxidation potentials close to the first four-electron wave, e.g. Cl_2(aq), Br_2(aq), were found to oxidize **5** smoothly, with the formation of the complex $[Mn(III)_3Mn(II)_6(Cl2poap\text{-}2H)_6](ClO_4)_9\cdot 7H_2O$ (**6**) as the major product in both cases. An X-ray structure of **6** revealed that the grid remained intact, but three of the corner manganese centers were oxidized to Mn(III), as indicated by substantially shortened Mn–L contacts [17,19,20]. Bulk electrolysis on **3** in acetonitrile produced the complex $[Mn(III)_4Mn(II)_5(2poap\text{-}2H)_6](ClO_4)_{10}\cdot 10H_2O$ (**7**), which was shown by X-ray crystallography to have a grid structure with all four corner Mn(II) centers oxidized to Mn(III) [20].

The plots of magnetic moment and susceptibility per mole as a function of temperature for **6** are shown in Fig. 20. A broad, shallow maximum appears at ~40–50 K in the susceptibility profile, which does not show up for **5**. This is a clear indication of intramolecular antiferromagnetic exchange. The room temperature moment is typical of the

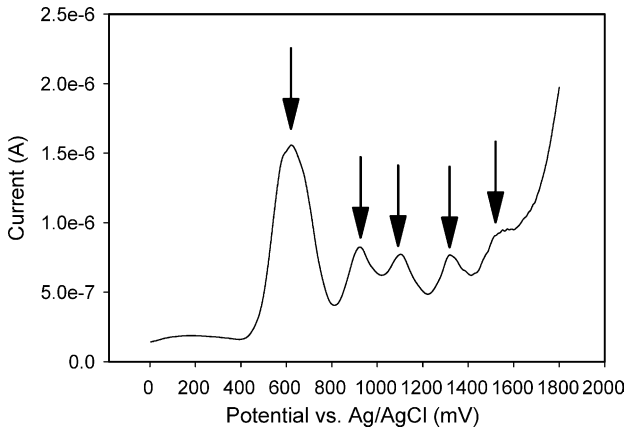

Fig. 19. Differential pulse voltammetry (CH_3CN vs. Ag/AgCl) for $[Mn_9(Cl2poap\text{-}2H)](ClO_4)_6\cdot 8H_2O$ (**5**).

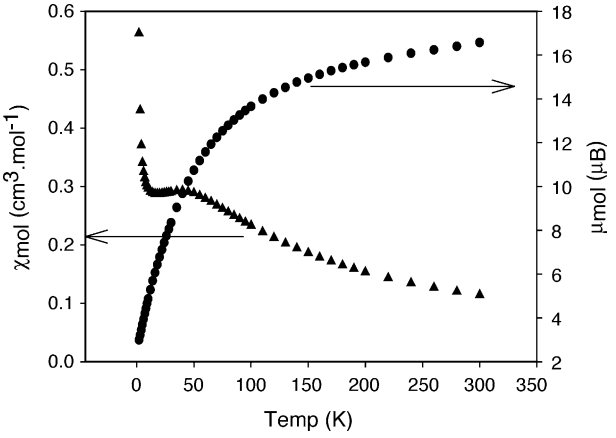

Fig. 20. Plots of molar susceptibility and magnetic moment as a function of temperature for $[Mn(III)_3Mn(II)_6(Cl2poap\text{-}2H)](ClO_4)_9{\cdot}7H_2O$ (**6**).

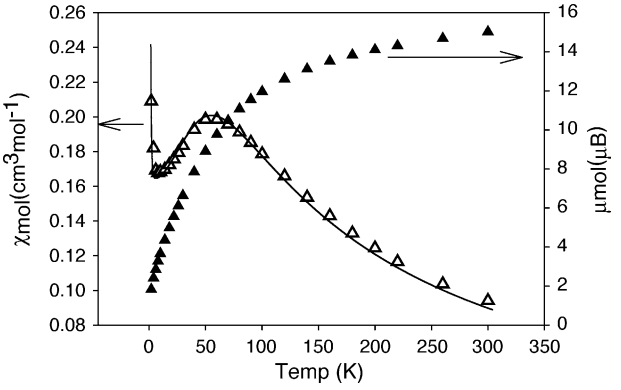

Fig. 22. Plots of molar susceptibility and magnetic moment as a function of temperature for $[Mn(III)_4Mn(II)_5(2poap\text{-}2H)](ClO_4)_{10}{\cdot}10H_2O$ (**7**). The solid line corresponds to a best comparison for $g = 2.0$, $J1 = J2 = -7\,cm^{-1}$ (see text).

Mn(II) grids as a whole, but the low temperature moment at 2 K (2.95 μ_B) is much lower than that observed for the parent compound, and is more typical of a system with two unpaired electrons ($S = 2/2$; e.g. Ni(II)). Magnetization versus field data (Fig. 21) show a near perfect fit for an $S = 2/2$ system at 2 K ($g = 2.0$) (solid line calculated using the appropriate Brillouin function for an $S = 2/2$ spin system). The divergence above 3.5 T is typical of the manganese grids as a whole, and is associated with a field dependent population of upper excited states in the complex spin manifold of the 42 electron grid [15].

The magnetic profile for **7** is shown in Fig. 22. The clear difference from **6** surrounds the appearance of a pronounced maximum in χ_{mol}, which is shifted to a higher temperature (~60 K), and the drop in moment at 2 K to 1.83 μ_B. The shift of the maximum in χ_{mol} to higher temperature signals enhanced exchange coupling, and the moment at 2 K is typical of a system with one unpaired electron ($S = 1/2$). Magnetization data as a function of field at 2 K confirm the ground state to be $S = 1/2$. The room temperature moments for **6** (16.3 μ_B) and **7** (15.3 μ_B) are indicative also of a reduced electron count in the grid, since typically for the $Mn(II)_9$ grids the moment exceeds 17 μ_B [20].

The ground state spins for **6** and **7** can be rationalized quite simply using Fig. 16. **6** has three corner $S = 4/2$ (Mn(III)) centers (e.g. 1, 3, 5), with the rest being Mn(II) ($S = 5/2$). Considering this spin subset for $J1 \approx J2$, in the antiferromagnetic low temperature limit, the ground state spin for the outer ring (1–8) would be 2/2. This corresponds to a ferrimagnetic system. Coupling of the 'ferrimagnetic' ring to the central metal ion would then lead to $S' = 5/2–3/2 = 2/2$ in the ground state, in agreement with observation. For compound **7**, with four corner $S = 4/2$ centers the resultant spin for the outer ring would be $4 \times 1/2$, which when coupled to the central metal ion would lead to an $S' = 5/2–2/2 = 1/2$, again in agreement with observation.

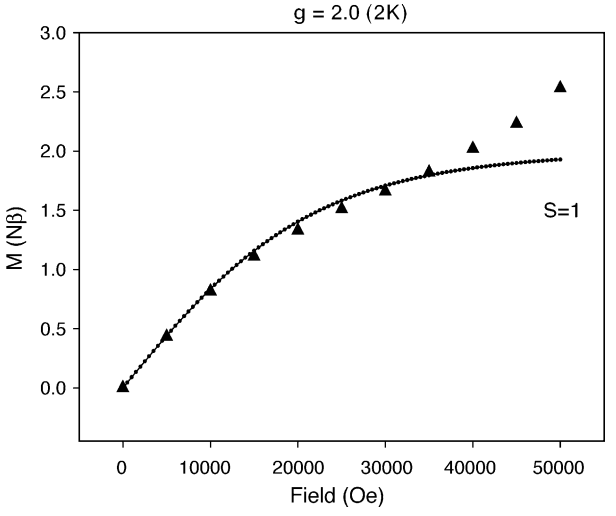

Fig. 21. Magnetization vs. field data for $[Mn(III)_3Mn(II)_6(Cl2poap\text{-}2H)](ClO_4)_9{\cdot}7H_2O$ (**6**) at 2 K.

7. Big spin systems—how to handle them?

7.1. Using lower dimensional systems to observe and rationalize trends

The largest matrix dimension for a fully isotropic calculation for the $Mn(II)_9$ grid ($S = 5/2$; $\sum S = 45/2$), including two J values (Fig. 16), is 88,900, which would require 60.3 GB of computer RAM (8 bit architecture). This is clearly beyond the capability of even very large work stations. For an $S = 4/2$ M_9 grid the largest dimension would be 25,200, requiring 5.1 GB. For an $S = 3/2$ grid the largest dimension is reduced to 5300, requiring only 225 MB of RAM. While it is therefore not possible to carry out a fully isotropic spin only calculation for the $Mn(II)_9$ grids, the novel spin properties of the grids, and an appreciation for the ground states of, e.g. the mixed oxidation state systems, can be obtained by using a grid with a lower dimensionality [15]. A $(d^3)_9$ system is a

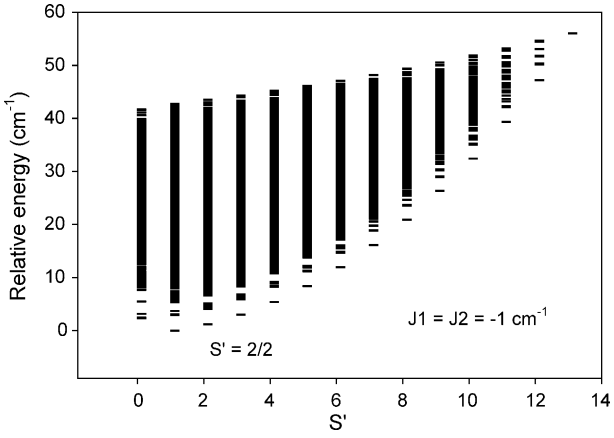

Fig. 23. Spin state energy spectrum for a $(d^2)(d^3)_8$ grid with $J1 = J2 = -1\ cm^{-1}$ (refer to Fig. 16).

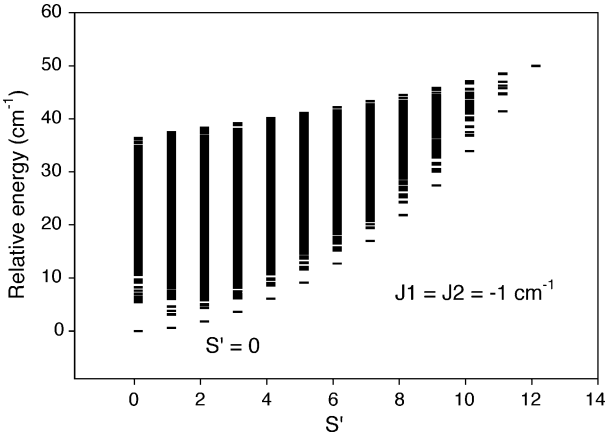

Fig. 25. Spin state energy spectrum for a $(d^2)_3(d^3)_6$ grid with $J1 = J2 = -1\ cm^{-1}$ (refer to Fig. 16).

useful comparative model, amenable to study with the average computer.

The $(d^3)_9$ case would be equivalent to the $(d^5)_9$ spin system in the sense that it has an odd number of spins and $S \neq 0$ ground state. For negative $J1$ the ground state for the outer ring would be $S = 0$, since there are an even number of spins. This then leads to an $S = 3/2$ ground state for the complex, regardless of the value of $J2$. Removing an electron from one corner site (e.g. 1 in Fig. 16; $(d^2)(d^3)_8$) clearly must now introduce spin interactions between the resultant spin in the ring, and the central ion. The total S'/energy profile for this system is shown in Fig. 23 (calculated using MAGMUN4.1), as a plot of S' against relative energy (energies calculated for $J1 = J2 = -1\ cm^{-1}$). The S' value with the lowest energy is $S' = 2/2$, which defines the ground state, and can be understood readily by considering the fact that the ring must have a ground state of $S' = 1/2$ in the low temperature antiferromagnetic limit, which would then couple with the central ion to give an $S' = 3/2–1/2 = 2/2$ ground state. Other similar plots are shown for $(d^2)_4(d^3)_5$ (Fig. 16; $1 = 3 = 5 = 7 = d^2$) and $(d^2)_3(d^3)_6$ (Fig. 16; $1 = 3 = 5 = d^2$) (Figs. 24 and 25, respectively), which by the same reasoning have ground states of $S' = 1/2$ and 0, respectively, in the low temperature antiferromagnetic limit. A plot of moment per mole for all four spin state combinations is illustrated in Fig. 26, which shows appropriate values for $S' = 0$, 1/2, 2/2, 3/2 for $J1 = J2 = -10\ cm^{-1}$.

The trends resulting from the theoretical substitutions of d^2 sites into a $(d^3)_9$ grid are directly applicable to the d^4 substituted $(d^5)_9$ grids **6** and **7**, and the ground states are in exact agreement with the general model, assuming that the outer ring and the central metal ion are treated as independent magnetic subunits.

7.2. *Symmetry reduction as a means of solving the exchange problem*

The square [3 × 3] grids are an ideal platform for symmetry reduction techniques in the spin state calculations, given the nominal four-fold symmetry which can be applied. D_4 symmetry would be appropriate assuming equivalent spin sites, and two J values (Fig. 16). Such an approach has

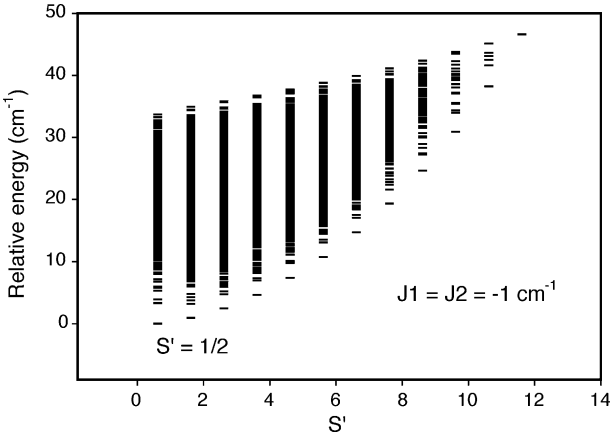

Fig. 24. Spin state energy spectrum for a $(d^2)_4(d^3)_5$ grid with $J1 = J2 = -1\ cm^{-1}$ (refer to Fig. 16).

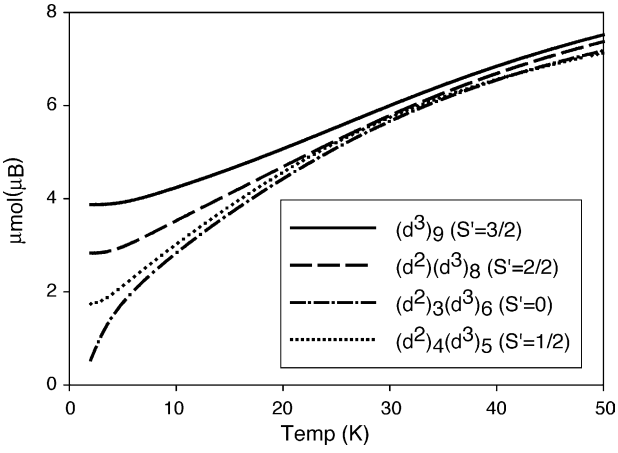

Fig. 26. Plot of moment per mole as a function of temperature for mixed spin state [3 × 3] grids with $S' = 0$, 1/2, 2/2, 3/2 ground states.

Table 1
Total spin quantum number states and symmetry assignments for a $(d^5)_9$ [3 × 3] grid calculated using imposed D_4 symmetry

$2S'$	$A1$	$A2$	$B1$	$B2$	E	∑ States
1	3373	3322	3350	3350	6690	26775
3	6414	6312	6363	6363	12726	50904
5	8847	8703	8772	8772	17526	70146
7	10468	10282	10375	10375	20750	83000
9	11224	11014	11121	11121	22210	88900
11	1142	10908	11025	11025	22050	88200
13	10379	10142	10258	10258	20484	82005
15	9108	8868	8988	8988	17976	71904
17	7578	7353	7467	7467	14898	59661
19	5970	5760	5865	5865	11730	46920
21	4474	4288	4379	4379	8730	34980
23	3168	3006	3087	3087	6174	24696
25	2133	1997	2066	2066	4108	16478
27	1350	1240	1295	1295	2590	10360
29	812	725	767	767	1520	6111
31	452	388	420	420	840	3360
33	239	192	216	216	422	1707
35	114	84	99	99	198	792
37	53	33	42	42	80	330
39	20	10	15	15	30	120
41	8	2	5	5	8	36
43	2	0	1	1	2	8
45	1	0	0	0	0	1

been demonstrated for square, hexanuclear and octanuclear ring structures, and relies on block factorizing the Hamiltonian matrix on the assumption that interchange of the spin sites meets the demands of the point group concerned [29]. Applying spin rotational and D_4 spatial symmetry the spin state spectrum for a $Mn(II)_9$ grid can be calculated. Table 1 shows the distribution of S' values (listed as $2S'$ for convenience), and their associated symmetries. The largest matrix dimension is 22,210 (E symmetry for $S' = 9/2$), which requires ∼3.9 GB of computer RAM. This is clearly beyond the capability of the average PC. It is of interest to note that there are 398,400 different energy states, many of which are degenerate.

However, the calculation has been completed for a $(d^4)_4(d^5)_5$ grid. Table 2 shows the S' values (listed as $2S'$ for convenience) and their energies, and the largest matrix dimension is 12,486, requiring ∼1.25 GB of RAM. A series of independent calculations has been carried out with several different $J1$ and $J2$ values in the range −0.1 to −10 K [30]. A first approximation to a fit based on a 'best' comparison of calculated magnetic profiles with the experimental data gives $g = 2.0$ and $J1 = J2 = -7.0\ cm^{-1}$. Experimental data for **7**, and a theoretical line for $J1 = J2 = -7.0\ cm^{-1}$ are shown in Fig. 22. Given the size of the spin state spectrum calculations, and the resulting complexity of the necessary non-linear regression analyses, it will be some time before a full fitting of the data for these systems can be achieved.

7.3. Larger grids

Limitations with total spin state calculations involve both S values at each spin center, and the number of spin sites.

Table 2
Total spin quantum number states and symmetry assignments for a $(d^4)_4(d^5)_5$ [3 × 3] grid calculated using imposed D_4 symmetry

$2S'$	$A1$	$A2$	$B1$	$B2$	E	∑ States
1	2032	1990	2011	2006	4013	16065
3	3828	3747	3794	3781	7575	30300
5	5212	5095	5162	5149	10291	41200
7	6052	5908	5991	5969	11960	47840
9	6340	6174	6263	6246	12486	49995
11	6100	5925	6025	6000	12025	48100
13	5482	5302	5402	5385	10757	43085
15	4603	4432	4529	4506	9035	36140
17	3647	3485	3571	3557	7103	28466
19	2704	2563	2642	2625	5267	21068
21	1897	1772	1840	1831	3648	14636
23	1240	1140	1195	1185	2380	9520
25	768	685	727	723	1436	5775
27	436	376	408	404	812	3248
29	235	189	213	212	415	1679
31	113	84	99	98	197	788
33	53	33	42	42	80	330
35	20	10	15	15	30	120
37	8	2	5	5	8	36
39	2	0	1	1	2	8
41	1	0	0	0	0	1

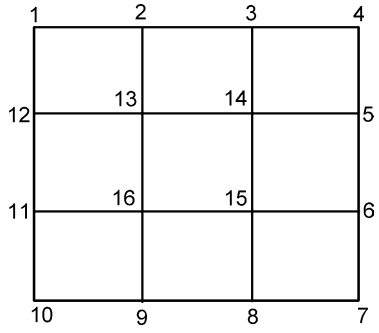

Fig. 27. Spin exchange model for [4 × 4] hexa-decanuclear grid.

The extended hexa-decanuclear [4 × 4] grid shown in Fig. 27 can be calculated easily for a Cu_{16} system, with 12,870 spin states (Table 3; $S = 1/2$; no imposed symmetry required). The complex exchange Hamiltonian (Eq. (14)) has 24 terms, and assuming an idealized situation, where the same exchange integral exists between each spin site connection, the energy

Table 3
Total spin quantum number states and symmetry assignments for a $(d^1)_{16}$ [4 × 4] grid

$2S'$	$A1$	$A2$	$B1$	$B2$	E	∑ States
0	209	169	201	171	340	1430
2	414	430	402	442	872	3432
4	484	440	468	456	896	3640
6	315	313	301	331	644	2548
8	175	149	161	159	308	1260
10	56	52	48	60	112	440
12	18	10	14	14	24	104
14	2	1	1	3	4	15
16	1	0	0	0	0	1

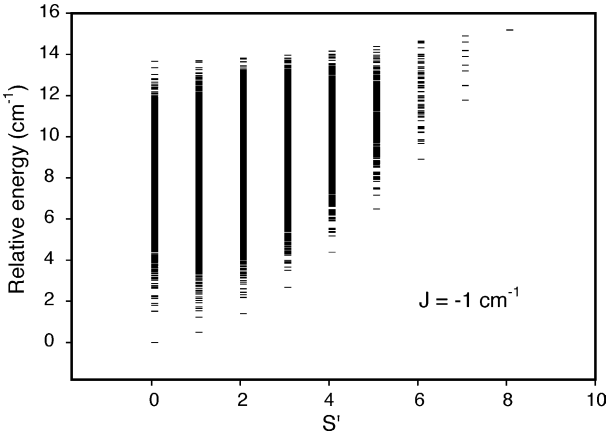

Fig. 28. Spin state energy spectrum for a [4 × 4] Cu_{16} grid.

profile (Fig. 28) would lead to a singlet ground state for negative J values.

$$\begin{aligned} H_{ex} = -J\{&S_1 \cdot S_2 + S_2 \cdot S_3 + S_3 \cdot S_4 + S_4 \cdot S_5 + S_5 \cdot S_6 \\ &+ S_6 \cdot S_7 + S_7 \cdot S_8 + S_8 \cdot S_9 + S_9 \cdot S_{10} + S_{10} \cdot S_{11} \\ &+ S_{11} \cdot S_{12} + S_1 \cdot S_{12} + S_{12} \cdot S_{13} + S_{13} \cdot S_{14} \\ &+ S_{14} \cdot S_{15} + S_{15} \cdot S_{16} + S_{16} \cdot S_{17} + S_2 \cdot S_{13} \\ &+ S_3 \cdot S_{14} + S_5 \cdot S_{14} + S_6 \cdot S_{15} + S_8 \cdot S_{15} \\ &+ S_9 \cdot S_{16} + S_{11} \cdot S_{16}\} \end{aligned} \quad (14)$$

Extending this approach to a comparable Ni_{16} [4 × 4] grid system ($S = 1$) leads to an enormous, and impractical calculation even with D_4 imposed symmetry, involving a total of 5,196,627 energy states. Diamagnetic Pb_{16} [4 × 4] grid complexes have recently been reported with 4,6-disubstituted pyrimidine based tetratopic ligands [31,32], and there is every reason to believe that paramagnetic analogues will be produced. However, it is clear that with what is a relatively simple grid system exchange coupling calculations will not be feasible with normal computers. Simple extension of the tritopic ligands based on poap (Fig. 1) and 2poap (Fig. 2), can be achieved by reaction of the precursor hydrazides with keto-esters, followed by elaboration with hydrazine and suitable terminating end groups. This would lead to tetratopic and pentatopic ligands, respectively, with [4 × 4] and [5 × 5] molecular grids as targets. Preliminary results indicate that pentatopic ligands can be synthesized by such routes [33].

8. Conclusion and outlook

Mn(II) grids and clusters based on polytopic picolylhydrazone ligands are a rich source of magnetic models, which provide a theoretical challenge for the solution of the intramolecular exchange problem when the spin state spectrum becomes too large for the average computer to handle. The manganese spin centers are bridged by deprotonated hydrazone oxygen atoms in [2 × 2], and [3 × 3] square grids, and in the trigonal bipyramidal $Mn(II)_5$ clusters, with large Mn–O–Mn angles (>125°), which lead to intramolecular antiferromagnetic exchange in all cases. The $Mn(II)_4$ and $Mn(II)_5$ exchange models can be fitted readily, and best fits achieved without computing difficulties. The $Mn(II)_9$ and mixed Mn(II)/Mn(III) nona-nuclear grids present a special challenge, which can be overcome using a computer with sufficient RAM. Current efforts using 2GB of RAM have been successful with the $(d^4)_4(d^5)_5$ case using D_4 spatial symmetry, but the RAM requirements for the $Mn(II)_9$ case (∼3.8 GB) indicate that dealing with such a large system will await the use of a much larger computer.

Exchange integrals (J) for the $Mn(II)_4$ and $Mn(II)_5$ systems are in the range −3 to −5 cm^{-1}. The oxidized $Mn(III)_4Mn(II)_5$ grid **7**, has a larger exchange coupling, which is consistent with the larger Mn–O–Mn angles. The extent of oxdidation in the mixed spin state [3 × 3] grids can be assessed readily through variable temperature and variable field magnetic studies, and as electrons are removed from the grid the spin states follow a logical sequence based on the exchange situation within the outer ring of metal ions, and the interaction of this ferrimagnetic ring with the central metal ion.

The use of convenient software packages for complex magnetic calculations simplifies the approach to understanding the magnetic properties of polynuclear spin-coupled clusters. However they have their own limitations. One current limitation with MAGMUN4.1 (written in MS Visual Basic) is the file size it can read. The current upper limit is 32768 energy states. Efforts are underway to increase this.

Acknowledgments

We thank the Natural Sciences and Engineering Research Council of Canada (NSERC) (L.K.T.), and EC-RTN-QUEMOLNA, contract #MRTN-CT-2003-504880 (O.W.), for financial support. A dedicated group of talented co-workers at Memorial University is also acknowledged, and in particular Liang Zhao, who was instrumental in developing this class of ligands, and the first Mn_9 grid complexes.

References

[1] R. Sessoli, D. Gatteschi, A. Caneschi, M.A. Novak, Nature (Lond.) 365 (1993) 141.
[2] E.K. Brechin, C. Boskovic, W. Wernsdorfer, J. Yoo, A. Yamaguchi, E.C. Sañudo, T.R. Concolino, A.L. Rheingold, H. Ishimoto, D.N. Hendrickson, G. Christou, J. Am. Chem. Soc. 124 (2002) 9710.
[3] M. Murugesu, J. Raftery, W. Wernsdorfer, G. Christou, E.K. Brechin, Inorg. Chem. 43 (2004) 4203.
[4] M. Soler, W. Wernsdorfer, K. Folting, M. Pink, G. Christou, J. Am. Chem. Soc. 126 (2004) 2156.
[5] L.K. Thompson, Coord. Chem. Rev. 233–234 (2002) 193.

[6] L.K. Thompson, O. Waldmann, Z. Xu, in: J.S. Miller, M. Drillon (Eds.), Magnetism: Molecules to Materials IV, Wiley–VCH, 2003, p. 173.
[7] M. Ruben, J. Rojo, F.J. Romero-Salguerro, L.H. Uppadine, J.-M. Lehn, Angew. Chem. Int. Ed. 43 (2004) 3644.
[8] C.J. Matthews, K. Avery, Z. Xu, L.K. Thompson, L. Zhao, D.O. Miller, K. Biradha, K. Poirier, M.J. Zaworotko, C. Wilson, A.E. Goeta, J.A.K. Howard, Inorg. Chem. 38 (1999) 5266.
[9] L.K. Thompson, C.J. Matthews, L. Zhao, Z. Xu, D.O. Miller, C. Wilson, M.A. Leech, J.A.K. Howard, S.L. Heath, A.G. Whittaker, R.E.P. Winpenny, J. Solid State Chem. 159 (2001) 308.
[10] C.J. Matthews, Z. Xu, S.K. Mandal, L.K. Thompson, K. Biradha, K. Poirier, M.J. Zaworotko, Chem. Commun. (1999) 347.
[11] C.J. Matthews, L.K. Thompson, S.R. Parsons, Z. Xu, D.O. Miller, S.L. Heath, Inorg. Chem. 40 (2001) 4448.
[12] L. Zhao, C.J. Matthews, L.K. Thompson, S.L. Heath, Chem. Commun. (2000) 265.
[13] L. Zhao, Z. Xu, L.K. Thompson, S.L. Heath, D.O. Miller, M. Ohba, Angew. Chem. Int. Ed. 39 (2000) 3114.
[14] O. Waldmann, R. Koch, S. Schromm, P. Müller, L. Zhao, L.K. Thompson, Chem. Phys. Lett. 332 (2000) 73.
[15] O. Waldmann, L. Zhao, L.K. Thompson, Phys. Rev. Lett. 88 (2002) 066401.
[16] L. Zhao, Z. Xu, L.K. Thompson, D.O. Miller, Polyhedron 20 (2001) 1359.
[17] L.K. Thompson, L. Zhao, Z. Xu, D.O. Miller, W.M. Reiff, Inorg. Chem. 42 (2003) 128.
[18] Z. Xu, L.K. Thompson, D.O. Miller, Polyhedron 21 (2002) 1715.
[19] L. Zhao, Z. Xu, H. Grove, V. Milway, L.N. Dawe, T.S.M. Abedin, L.K. Thompson, T.L. Kelly, D.O. Miller, L. Weeks, J.G. Shapter, K.J. Pope, Inorg. Chem. 43 (2004) 3812.
[20] L.K. Thompson, T.L. Kelly, L.N. Dawe, H. Grove, M.T. Lemaire, J.A.K. Howard, E.C. Spencer, C.J. Matthews, S.T. Onions, S.J. Coles, P.N. Horton, M.B. Hursthouse, M.E. Light, Inorg. Chem. 43 (2004) 7605.
[21] K. Kambe, J. Phys. Soc. Jpn. 5 (1950) 48.
[22] MAGMUN/OW0L is available as a combined package (MAGMUN4.1) free of charge from the authors (lthomp@mun.ca; oliver.waldmann@iac.unibe.ch). MAGMUN4.1 has been developed by Dr. Zhiqiang Xu (Memorial University), and OW01.exe by Dr. O. Waldmann. Source codes are not distributed. The programs may be used only for scientific purposes. If either routine is used to obtain publishable scientific results, the origin of the programs, and a reference to this review, should be quoted.
[23] R.L. Martin, in: E.A.V. Ebsworth, A.G. Maddock, A.G. Sharpe (Eds.), New Pathways in Inorganic Chemistry, Cambridge University Press, Cambridge, 1978, Chapter 9.
[24] K.S. Murray, Adv. Inorg. Chem. 43 (1995) 261–356.
[25] D. Gatteschi, L. Pardi, Gazz. Chim. Ital. 123 (1993) 231.
[26] J.J. Borrás-Almenar, J.M. Clemente-Juan, E. Coronado, B.S. Tsukerblat, J. Comput. Chem. 22 (2001) 985.
[27] M.E. Fisher, Am. J. Phys. 32 (1964) 343.
[28] T. Guidi, S. Carretta, P. Santini, E. Liviotti, N. Magnani, C. Mondelli, O. Waldmann, L.K. Thompson, L. Zhao, C.D. Fost, G. Amoretti, R. Caciuffo, Phys. Rev. B 69 (2004) 104432.
[29] O. Waldmann, Phys. Rev. B 61 (2000) 6138.
[30] O. Waldmann, L.K. Thompson, D.W. Thompson, T.L. Kelly, unpublished results.
[31] M. Barboiu, G. Vaughan, R. Graff, J.-M. Lehn, J. Am. Chem. Soc. 125 (2003) 10257.
[32] S.T. Onions, A.M. Franklin, P.N. Norton, M.B. Hursthouse, C.J. Matthews, Chem. Commun. (2003) 2864.
[33] T.S.M. Abedin, V. Niel, L.K. Thompson, unpublished results.